PCCP

PAPER

View Article Online
View Journal | View Issue

Cite this: *Phys. Chem. Chem. Phys.*, 2018, **20**, 16266

Hydrogenation properties of lithium and sodium hydride – *closo*-borate, $[B_{10}H_{10}]^{2-}$ and $[B_{12}H_{12}]^{2-}$, composites†

Steffen R. H. Jensen,[a] Mark Paskevicius,[a] Bjarne R. S. Hansen,[a] Anders S. Jakobsen,[a] Kasper T. Møller,[a] James L. White,[b] Mark D. Allendorf,[b] Vitalie Stavila,*[b] Jørgen Skibsted[c] and Torben R. Jensen*[a]

The hydrogen absorption properties of metal *closo*-borate/metal hydride composites, $M_2B_{10}H_{10}$–8MH and $M_2B_{12}H_{12}$–10MH, M = Li or Na, are studied under high hydrogen pressures to understand the formation mechanism of metal borohydrides. The hydrogen storage properties of the composites have been investigated by *in situ* synchrotron radiation powder X-ray diffraction at $p(H_2)$ = 400 bar and by *ex situ* hydrogen absorption measurements at $p(H_2)$ = 526 to 998 bar. The *in situ* experiments reveal the formation of crystalline intermediates before metal borohydrides (MBH_4) are formed. On the contrary, the $M_2B_{12}H_{12}$–10MH (M = Li and Na) systems show no formation of the metal borohydride at T = 400 °C and $p(H_2)$ = 537 to 970 bar. ^{11}B MAS NMR of the $M_2B_{10}H_{10}$–8MH composites reveal that the molar ratio of $LiBH_4$ or $NaBH_4$ and the remaining B species is 1 : 0.63 and 1 : 0.21, respectively. Solution and solid-state ^{11}B NMR spectra reveal new intermediates with a B : H ratio close to 1 : 1. Our results indicate that the $M_2B_{10}H_{10}$ (M = Li, Na) salts display a higher reactivity towards hydrogen in the presence of metal hydrides compared to the corresponding $[B_{12}H_{12}]^{2-}$ composites, which represents an important step towards understanding the factors that determine the stability and reversibility of high hydrogen capacity metal borohydrides for hydrogen storage.

Received 17th November 2017,
Accepted 24th May 2018

DOI: 10.1039/c7cp07776a

rsc.li/pccp

Introduction

The human consumption of energy has increased over the past decades, and has mainly been covered by burning fossil fuels at an increasing rate, which has led to an increase in CO_2 levels in the atmosphere.[1,2] Despite an abundance of available renewable energy from sun and wind, these energy sources are intermittent and fluctuate over time and geography. Thus, energy storage is required to compensate for the variability in renewable energy fluxes, and hydrogen is a promising energy carrier with the highest gravimetric energy density among all known compounds (ρ_m = 120 MJ kg^{-1}).[3] However, compressed hydrogen gas has a low volumetric energy density (ρ_V = 8.5 MJ L^{-1}). The volumetric density can be improved by storing hydrogen in a solid, for example in reversible metal hydrides.[3–5] Metal borohydrides have been proposed as solid-state hydrogen storage media due to their high hydrogen content and potential reversibility.[6–9] The challenge of using metal borohydrides as hydrogen carriers is that they often possess high hydrogen release temperatures, coupled with harsh conditions needed for hydrogenation.[10–14] These issues have generated interest in the synthesis and investigation of hydrogen storage properties of bi- and tri-metallic main group/transition metal borohydrides with tunable hydrogen desorption temperatures.[15–21] Another approach has been to stabilize unstable borohydrides *e.g.* $Fe(BH_4)_2$ and $Co(BH_4)_2$, using ammonia.[22] Reactive hydride composites have also been used to thermodynamically destabilize metal borohydrides by altering the decomposition mechanism, *e.g.* $LiBH_4$–MgH_2, or by changing the morphology of the sample, *e.g.* $NaBH_4$–KBH_4, where the solid is transformed into a liquid.[23,24] Finally, several materials have been studied as catalysts for hydrogen uptake and release, *e.g.*, transition metals and their halides and oxides.[25–27] However, to the best of our knowledge, an efficient catalyst for breaking and forming B–H bonds has not yet been discovered.

[a] *Center for Materials Crystallography, Interdisciplinary Nanoscience Center (iNANO) and Department of Chemistry, Aarhus University, Langelandsgade 140, 8000 Aarhus C, Denmark. E-mail: trj@chem.au.dk*
[b] *Chemistry, Combustion, and Materials Center, Sandia National Laboratories, Livermore, California 94551, USA. E-mail: vnstavi@sandia.gov*
[c] *Department of Chemistry and Interdisciplinary Nanoscience Center (iNANO), Aarhus University, Langelandsgade 140, 8000 Aarhus C, Denmark*

† Electronic supplementary information (ESI) available. See DOI: 10.1039/c7cp07776a

Polyhydro-*closo*-polyborates (also known as *closo*-borates), $B_nH_n^{2-}$ (n = 6–12), are anions comprised of boron atoms with solely terminal hydrogen in closed polyhedral clusters. These compounds can be prepared through a variety of solid-state and solution synthetic approaches.[28] Higher *closo*-borates, such as dodecahydro-*closo*-dodecaborates ($[B_{12}H_{12}]^{2-}$ salts) and decahydro-*closo*-decaborates ($[B_{10}H_{10}]^{2-}$ salts) are often assumed to be intermediates in the mechanism for hydrogen release and uptake in metal borohydrides, $M(BH_4)_x$, and their relatively high stability may retard the reversibility of these reactions.[28–31] The formation of higher *closo*-borates during decomposition of metal borohydrides may occur in a reaction between the metal borohydride and transient diborane (B_2H_6). The formation of either $Li_2B_{10}H_{10}$ or $Li_2B_{12}H_{12}$, depending on temperature, has clearly been observed by mechano-chemical treatment of $LiBH_4$ in a diborane atmosphere.[32] The formation of $Li_2B_{12}H_{12}$ is also observed for the reactive hydride composite, $LiBH_4$–MgH_2–Al, which shows decreasing reversible hydrogen content commensurate with increasing amounts of $Li_2B_{12}H_{12}$ during cycling of hydrogen release and uptake.[30] In a similar manner, magnesium borohydride, $Mg(BH_4)_2$, decomposes under vacuum at $T \approx 200$ °C and forms *arachno*-$Mg(B_3H_8)_2$, which can absorb hydrogen at more moderate conditions, *e.g.*, $p(H_2)$ = 120 bar and T = 250 °C, in contrast to the *closo*-borates.[33]

Hydrogen release and absorption reactions in boron-based hydrides remain not fully understood. Density functional theory (DFT) calculations have been used to predict reaction enthalpies for multiple chemical reactions that reversibly store hydrogen and to identify promising reactions with large storage capacities and relevant thermodynamic properties.[34,35] Experiments have revealed that $LiBH_4$ decomposes into LiH and B, with $Li_2B_{12}H_{12}$ as an intermediate phase. Theoretical work has suggested formation of $(LiBH_4)_n$, $n \leq 12$, nanoclusters, which decompose into mixed Li_nB_n clusters *via* a series of intermediate clusters of $Li_nB_nH_m$, ($m \leq 4n$).[36] A variety of other intermediates have also been suggested, with the $[B_{12}H_{12}]^{2-}$ as the most stable, which is considered to hamper hydrogen uptake reactions.[37,38] Experimental determination of structure and composition of intermediates is often hampered by poor crystallinity and difficulties in preparation of phase-pure samples.

Recently, $M_2B_{12}H_{12}$–10MH composites were hydrogenated at $p(H_2)$ = 1000 bar and 500 °C for 72 hours forming the corresponding metal borohydrides, MBH_4, M = Li, Na or K.[39] This has prompted the present hydrogenation study of *closo*-polyborate-containing composites, $M_2B_{10}H_{10}$–8MH and $M_2B_{12}H_{12}$–10MH, M = Li or Na, using less harsh conditions in custom-made hydrogenation equipment designed to monitor the hydrogen uptake.[40] In doing so, the reaction pathway and kinetic issues associated with the hydrogenation of *closo*-borate containing samples can be assessed. It is expected that this information will provide insights into the "boron-sink" *closo*-borates in borohydride-based hydrogen storage systems. The mechanism for hydrogen uptake is investigated using *in situ* synchrotron radiation powder X-ray diffraction (SR-PXD), *ex situ* powder X-ray diffraction (PXD), Fourier transform infrared spectroscopy (FT-IR), as well as solution and solid-state ^{11}B NMR and ^{23}Na magic-angle spinning (MAS) NMR.

Experimental

Sample preparation

Lithium hydride, LiH (Sigma-Aldrich, 95%), and sodium hydride, NaH (Sigma-Aldrich, 95%), were used as supplied. Anhydrous $Li_2B_{10}H_{10}$ and $Na_2B_{10}H_{10}$ were synthesized from decaborane ($B_{10}H_{14}$, Katchem), dimethyl sulfide, liquid ammonia and the respective hydroxides MOH, using a method described elsewhere.[41] $Li_2B_{12}H_{12}{\cdot}4H_2O$ and $Na_2B_{12}H_{12}{\cdot}xH_2O$ (Katchem) were heated to 245 °C under dynamic vacuum for 12 hours to remove coordinated water. The *closo*-borates $M_2B_{10}H_{10}$ or $M_2B_{12}H_{12}$ were mixed with metal hydrides MH, M = Li or Na, in the molar ratio 1 : 8 or 1 : 10, respectively, to form a composite with a M : B ratio of 1 : 1. The mixtures were then manually ground for 3 minutes. These samples are denoted Li_2B_{10}-A, Li_2B_{12}-A, Na_2B_{10}-A and Na_2B_{12}-A. Other samples were prepared with either 3 minutes of manual grinding (Li_2B_{12}-As and Na_2B_{12}-As) or 15 minutes of ball-milling (ball to powder ratio of 25 : 1) (Li_2B_{10}-Ab, Na_2B_{10}-Ab, Li_2B_{10}-Ab and Na_2B_{12}-Ab). All handling of the chemicals was performed in an argon-filled glovebox with $p(O_2, H_2O) < 1$ ppm.

The *closo*-borate-hydride composites (Li_2B_{10}-A, Li_2B_{12}-A, Na_2B_{10}-A and Na_2B_{12}-A) were hydrogenated in custom-made equipment by loading the mixed powders (80–200 mg) into a steel container, which is closed with a filter and placed in a specialized sample cell.[42] High pressures (HP) are generated using a metal hydride hydrogen compressor, *i.e.* heating a commercial AB_5 hydrogen storage alloy with the composition $MmNi_{4.35}Co_{0.8}Al_{0.05}$ where Mm is a mixture of rare earth metals, primarily La and Ce. The pressure generated at room temperature, $p(H_2) \sim 400$ bar, was increased to 526–547 bar during heating to either ~300 or ~400 °C ($\Delta T/\Delta t$ = 5 °C min^{-1}) and was then kept isothermal for 24 hours. The high-pressure hydrogenation experiments were performed at 400 °C under hydrogen pressures of 970 to 998 bar in a stainless steel reactor. An overview of the hydrogen-treated samples is given in Table 1.

Characterization

In-house powder X-ray diffraction (PXD). In-house powder X-ray diffraction patterns were measured on a Rigaku Smart Lab diffractometer using a Cu source and conversion beam mirror (Cu $K_{\alpha 1}$ radiation, λ = 1.540593 Å). Data were collected in the 2θ range 5° to 50° at 3° min^{-1} using a Rigaku D/tex detector. Samples were placed in 0.5 mm boron silicate capillaries and sealed with grease under argon in a glovebox.

Fourier transform infrared spectroscopy (FT-IR). All samples were characterized by FT-IR using a NICOLET 360 FT-IR from Thermo Electron Corporation. Data were measured in the range 4000–400 cm^{-1} and 32 scans, with a spectral resolution of 4 cm^{-1}, were collected per sample and averaged. The samples were briefly exposed to air (~10 s) prior to measurement.

Synchrotron radiation powder X-ray diffraction. *In situ* synchrotron radiation powder X-ray diffraction (SR-PXD)

Table 1 Overview of the hydrogenated samples. The total pressure allows calculation of hydrogen H_2 uptake ($\Delta m/m$). Unidentified compounds are denoted, **1**, **2**, **3**, or **4**

Name	Ratio $M_2B_{10/12}H_{10/12}$: MH, M = Li or Na	Synthesis, hydrogenation of sample	T [°C]	$p(H_2)_{start}$ [bar]	$p(H_2)_{end}$ [bar]	$\Delta m/m$ [wt% H_2]	Time [h]	Products
Li_2B_{10}-B	1 : 8	Li_2B_{10}-A	307	526	516	2.9	24	$LiBH_4$ + LiH + **1**
Li_2B_{10}-C	1 : 8	Li_2B_{10}-Ab	400	998	773[a]	—	48	$LiBH_4$ + LiH
Li_2B_{12}-B	1 : 10	Li_2B_{12}-A	402	547	540	2.2	24	$Li_2B_{12}H_{12}$ + LiH
Li_2B_{12}-C	1 : 10	Li_2B_{12}-Ab	400	970	955	—	48	$Li_2B_{12}H_{12}$ + LiH
Li_2B_{12}-D	1 : 10	Li_2B_{12}-As	400	970	955	—	48	$Li_2B_{12}H_{12}$ + LiH
Na_2B_{10}-B	1 : 8	Na_2B_{10}-A	289	534	527	3.2	24	$NaBH_4$ + NaH + **2**
Na_2B_{10}-C	1 : 8	Na_2B_{10}-Ab	400	998	773[a]	—	48	$NaBH_4$ + NaH
Na_2B_{12}-B	1 : 10	Na_2B_{12}-A	401	536	533	1.5	24	$Na_2B_{12}H_{12}$ + NaH + **3** + **4**
Na_2B_{12}-C	1 : 10	Na_2B_{12}-Ab	400	970	955	—	48	$Na_2B_{12}H_{12}$ + NaH
Na_2B_{12}-D	1 : 10	Na_2B_{12}-As	400	970	955	—	48	$Na_2B_{12}H_{12}$ + NaH

[a] Vessel had a ~4 bar h^{-1} leak, leading to a large decrease in pressure over the course of the experiment.

measurements were conducted at beam line P02.1 at the synchrotron facility PETRA III, DESY, Germany, with a high photon energy of 60 keV, λ = 0.20775 Å. The data were collected using a fast area detector from Perkin Elmer (XRD1621) and an X-ray exposure time of 10 seconds per diffraction pattern. The high photon energy is required to penetrate the thick-walled sapphire capillaries (o.d. = 3.0 mm, i.d. = 0.8 mm) that are necessary when working at high pressure ($p(H_2) > 200$ bar). For the high pressure measurement, a modified high pressure cell is used as described previously.[40] The *in situ* hydrogenation was performed by increasing the hydrogen pressure to 407–440 bar at room temperature (RT), followed by heating to 300 °C for the $M_2B_{10}H_{10}$–8MH composites and 400 °C for the $M_2B_{12}H_{12}$–10MH composites with a heating and cooling rate of $\Delta T/\Delta t$ = 10 °C min^{-1}. The *in situ* HP SR-PXD experiment for $Li_2B_{10}H_{10}$–8LiH was conducted for ~12 hours, whereas the experiments for $Na_2B_{10}H_{10}$–8NaH and $Na_2B_{12}H_{12}$–10NaH were conducted for ~4 hours.

NMR spectroscopy. The solid-state ^{11}B and ^{23}Na MAS NMR spectra were acquired on a Bruker AVANCE-700 spectrometer (16.4 T) using a triple-tuned ^1H-X-Y 4 mm MAS probe and a spinning speed of ν_R = 15.0 kHz. The ^{11}B NMR experiments employed a 0.5 μs excitation pulse ($\gamma B_1/2\pi$ = 62 kHz), ^1H SPINAL-64 decoupling ($\gamma B_2/2\pi$ = 100 kHz) and a relaxation delay of 10 s. The ^{23}Na spectra were acquired with a 0.5 μs excitation pulse ($\gamma B_1/2\pi$ = 60 kHz) and a 10 s relaxation delay. The solution ^{11}B NMR spectra were obtained on a Varian Direct Drive VNMRS-600 spectrometer (14.1 T) using a 4 mm CP/MAS probe for solids, no sample spinning, and ^1H decoupling ($\gamma B_2/2\pi$ = 50 kHz). All samples were packed in airtight end-capped zirconia rotors in an argon-filled glovebox. Solutions for ^{11}B NMR measurements were prepared by dissolving 20–40 mg of sample in dry tetrahydrofuran (THF). ^{11}B and ^{23}Na chemical shifts are relative to neat $F_3B{\cdot}O(CH_2CH_3)$ and a 0.1 M aqueous solution of NaCl, respectively.

Results and discussion

Hydrogenation of metal decahydro-*closo*-decaborate $M_2B_{10}H_{10}$-8MH compositions

Sample $Li_2B_{10}H_{10}$–8LiH. The Li_2B_{10}-A sample was heated to 307 °C ($\Delta T/\Delta t$ = 5 °C min^{-1}) and kept isothermal for 24 hours at $p(H_2)_{start}$ = 526 bar, Fig. S1 (ESI†). The hydrogen pressure decreased slowly, 0.054 wt% per h, for the first 6 hours, then ~5× faster (0.262 wt% per h) for 8 hours, and again slower for the remaining 8 hours, suggesting that there was an incubation period before hydrogen absorption could proceed rapidly or that several reactions take place. The pressure decrease corresponds to a total uptake of 2.9 wt% H_2, which is about 4× less than the theoretical hydrogen uptake, *i.e.* 11.3 wt%, which would correspond to full conversion of the sample to $LiBH_4$. PXD of the post-hydrogenation sample, Li_2B_{10}-B (Fig. 1), reveals that the reactants, $Li_2B_{10}H_{10}$ and LiH, are almost completely consumed during the formation of $LiBH_4$ and **1**. PXD of Li_2B_{10}-A treated at 400 °C, $p(H_2)$ = 998 bar H_2 for 48 h (Li_2B_{10}-C) (Fig. S2, ESI†) also reveals the formation of $LiBH_4$ and intermediate **1**. However, additional Bragg reflections appear at low Bragg angles (2θ), which are assigned to impurities from the reaction vessel. Compound **1** has not previously been reported and may be an intermediate in the formation of $LiBH_4$ with a lithium/boron ratio in between $Li_2B_{10}H_{10}$ and $LiBH_4$, *i.e.*, 0.2 < Li/B < 1. Observed Bragg diffraction data,

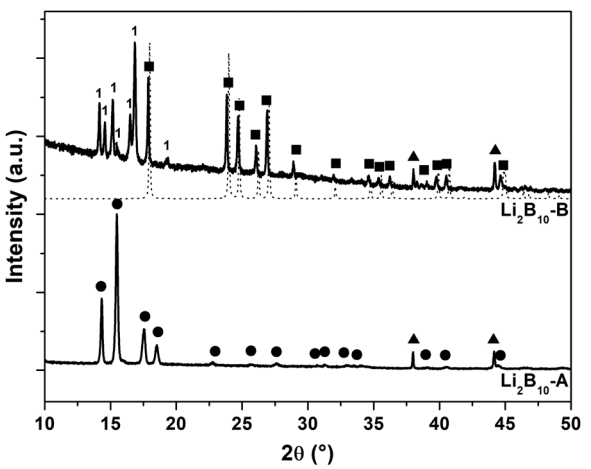

Fig. 1 Normalized powder X-ray diffraction patterns of $Li_2B_{10}H_{10}$–8LiH after manually grinding (Li_2B_{10}-A) and after hydrogenation (Li_2B_{10}-B) at T = 307 °C and $p(H_2)$ = 526 bar for 24 hours (λ = 1.540593 Å). Symbols: ■ o-$LiBH_4$, ● $Li_2B_{10}H_{10}$, ▲ LiH, and compound **1**. The dotted pattern is that of pure $LiBH_4$, overlaid for comparison.

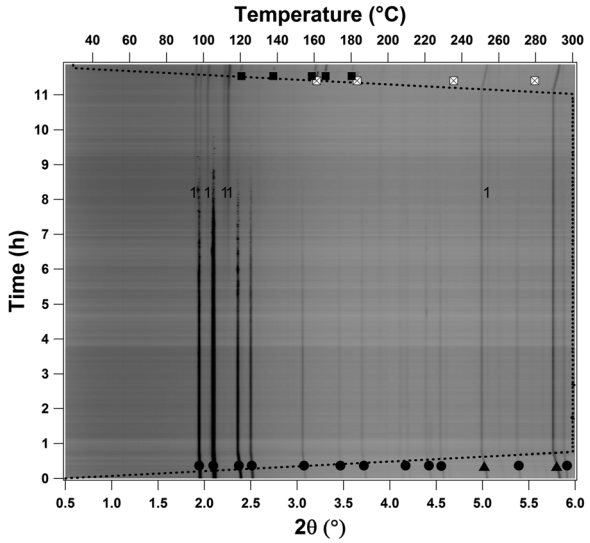

Fig. 2 *In situ* high pressure synchrotron powder X-ray diffraction patterns of the hydrogenation of $Li_2B_{10}H_{10}$–8LiH heated from RT to 300 °C, at $p(H_2)$ = 407 bar ($\Delta T/\Delta t$ = 10 °C min^{-1}, λ = 0.20720 Å). The sample was kept isothermal at T = 300 °C for ~10 hours. The dashed line indicates the temperature profile. Symbols: ■ o-$LiBH_4$, ⊠ h-$LiBH_4$, ● $Li_2B_{10}H_{10}$, ▲ LiH, and compound **1**.

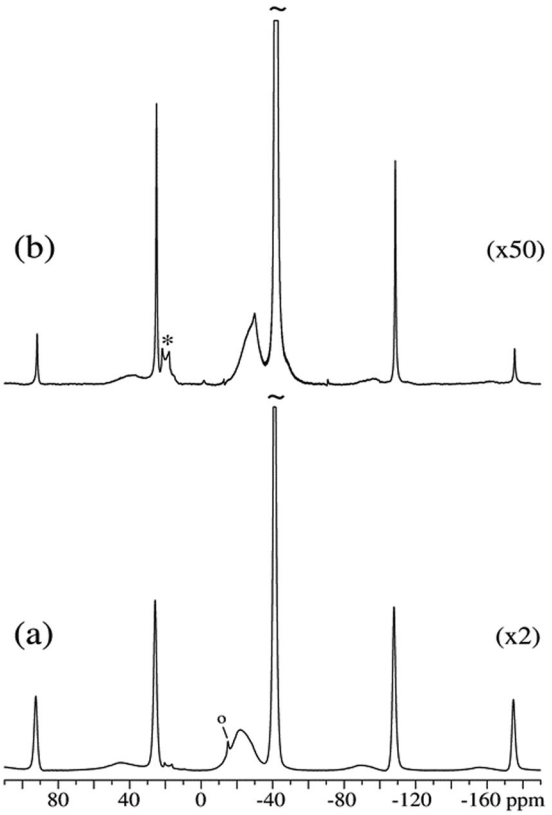

Fig. 3 ^{11}B MAS NMR spectra (16.45 T, ν_R = 15.0 kHz) of the hydrogenated samples (a) Li_2B_{10}-B and (b) Na_2B_{10}-B. The centerbands for $LiBH_4$ and $NaBH_4$ are cut-off at 1/2 and 1/50 of their total heights in (a) and (b), respectively. The asterisk indicates the second-order quadrupole lineshape from a minor impurity of BO_3 species (identified for both samples), most likely produced prior to the NMR experiments, whereas the open circle in (a) identifies a centerband at −15.1 ppm (0.7% of the boron in the sample) from a small amount of $Li_2B_{12}H_{12}$ in the sample.

d-spacings and relative intensities, from **1** are listed in Table S1 (ESI†), which can be indexed with an orthorhombic unit cell, a = 6.0754(2), b = 6.2494(2), c = 21.019(5) Å, V = 778.0(3) Å^3.

The hydrogenation of $Li_2B_{10}H_{10}$–8LiH was further studied by *in situ* SR-PXD at high hydrogen pressure, $p(H_2)$ = 407 bar, and isothermal conditions, T = 300 °C (Fig. 2). The PXD signatures of the reactants, $Li_2B_{10}H_{10}$ and LiH, were observed at RT, after ~6 hours the unidentified compound **1** emerged in accordance with *ex situ* PXD (Fig. 1 and Table S1, ESI†), and reflections from $Li_2B_{10}H_{10}$ completely disappeared after ~9 hours. This agrees with the induction period observed in Fig. S1 (ESI†). As Bragg reflections from $Li_2B_{10}H_{10}$ disappear, the reflections from **1** become more pronounced. After ~11 hours the sample is cooled and crystallization of h-$LiBH_4$ (h-hexagonal) is observed (T_{melt} = 280 °C), which transforms into the ambient o-$LiBH_4$ polymorph (o-orthorhombic).[12,43] This indicates that **1** may be an intermediate in the formation of $LiBH_4$.

The ^{11}B MAS NMR spectrum of Li_2B_{10}-B is dominated by the narrow centerband resonance at −41.1 ppm from $LiBH_4$ (Fig. 3a). In addition, a somewhat broader centerband is observed at −23 ppm, which is ascribed to boron in compound **1**, since the resonance does not match with the chemical shift reported for $Li_2B_{10}H_{10}$ at −28.8 ppm.[44] All spinning sidebands for the central and satellite transitions are observed for $LiBH_4$ whereas only a part of the spinning sideband manifold from the satellite transitions is observed for compound **1**. Thus, the total intensity for the ^{11}B central and satellite transitions for $LiBH_4$ is obtained as the sum of intensities for the centerband and all spinning sidebands, whereas the central-transition intensity for compound **1** is obtained from the intensities for the centerband and first-order spinning sidebands after an intensity correction to these peaks from the contribution from the satellite transitions. The central-transition intensity for $LiBH_4$ is obtained as 4/10 of the total intensity, which holds for a spin 3/2 nucleus, and comparison of this value with the central transition intensity for **1** reveals that the molar ratio for boron in $LiBH_4$ and **1** is 1 : 0.63, which corresponds to an uptake of 2.8 wt% H_2, matching well with the observed hydrogenation, 2.9 wt% H_2.[44] This indicates that the absorbed hydrogen only goes toward producing $LiBH_4$ as the B : H ratio in the unknown compound **1** is 1 : 1, consistent with a higher borate, which is also reflected in its characteristic IR mode and ^{11}B chemical shift. Thus, ^{11}B MAS NMR reveals that all $Li_2B_{10}H_{10}$ (−0.9 ppm and −28.8 ppm) is consumed during hydrogenation and that $LiBH_4$ and **1** are the only reaction products, besides a minor amount of a BO_3 species (~20 ppm), corresponding to 3.5% of the boron in the sample. Solution-state ^{11}B NMR spectra of Li_2B_{10}-B dissolved in THF obtained without and with ^{1}H decoupling (Fig. S4, ESI†) allow identification of resonances at −14.0 ppm ($^1J_{BH}$ = 142 Hz), −15.6 ppm ($^1J_{BH}$ = 120 Hz), −16.0 ppm ($^1J_{BH}$ = 120 Hz), −16.7 ppm ($^1J_{BH}$ = 120 Hz), −18.0 ppm ($^1J_{BH}$ = 150 Hz) and −20.7 ppm ($^1J_{BH}$ = 142 Hz) in addition to the main peak at −41.8 ppm from the $[BH_4]^-$ units.

All resonances in the −14.0 to −20.7 ppm region show doublets in the ^{1}H-coupled spectra, demonstrating that they originate from boron sites which are directly bonded to one H atom. The resonance and $^{1}J_{BH}$ coupling at −15.6 ppm is in agreement with the ^{11}B NMR data reported for $[B_{12}H_{12}]^{2-}$,[45] matching the impurity of $Li_2B_{12}H_{12}$ in the solid-state ^{11}B NMR spectrum (Fig. 3a). The remaining resonances, and, in particular, the peak at −20.7 ppm, may originate from the unknown compound **1** and thereby suggest that this phase contains boron sites directly bonded to a single H atom. Moreover, comparison of the ^{11}B chemical shifts with those reported for relevant borate species (Table S4, ESI†) strongly suggests that compound **1** contains *closo*-borate units.

The formation of $LiBH_4$ is also confirmed by FT-IR (Fig. S3, ESI†). The IR spectrum of Li_2B_{10}-A has a single large B–H stretching mode at 2500 cm^{-1} with minor modes at lower wavenumbers consistent with metal *closo*-borates.[46,47] For Li_2B_{10}-B, the B–H stretching mode at 2500 cm^{-1} has almost disappeared while B–H stretching modes appear around 2300 cm^{-1}, which correspond to those of $LiBH_4$.[48,49]

This work suggests that **1** has a lithium–boron ratio in between $Li_2B_{10}H_{10}$ and $LiBH_4$, *i.e.* 0.2 < Li/B < 1, and a hydrogen–boron ratio close to 1:1. A hydrogen uptake of 2.9 wt% H_2 was measured, which corresponds to a sample composition of 10Li–10B–23.6H. After hydrogenation, the sample contains $LiBH_4$ and LiH and, therefore, also some metal borates richer in boron and hydrogen than lithium. However, the spectroscopy and diffraction data do not unambiguously identify any such compounds.

Sample $Na_2B_{10}H_{10}$–8NaH. Hydrogenation of Na_2B_{10}-A was conducted at T = 289 °C and $p(H_2)$ = 534 bar and kept isothermal for 24 hours, Fig. S5 (ESI†). The hydrogen pressure was steady for the first 3 hours at $p(H_2)$ = 534 bar, then decreased, at 0.248 wt% per h, over the next 12 h, and then more slowly at 0.091 wt% per h during the remaining 8 hours (Fig. S5, ESI†). This reveals an induction period of 3 h prior to absorption of 3.2 wt% H_2, which is approximately half of the theoretical maximum, *i.e.* 6.23 wt%, which would correspond to full conversion to $NaBH_4$.

PXD of Na_2B_{10}-B reveals Bragg reflections from $NaBH_4$ along with an unidentified compound, denoted **2**, and some unreacted NaH (Fig. 4). PXD of the high-pressure sample, Na_2B_{10}-C, reveals that $NaBH_4$ is the major crystalline product, along with **2** (Fig. S6, ESI†). The new compound **2** has reflections at low Bragg angles $2\theta < 7^\circ$ ($d > 13$ Å) (Table S2, ESI†), which can be indexed with a relatively large monoclinic unit cell, a = 12.7068(5), b = 23.3384(7), c = 16.8802(8) Å, β = 105.456(4)°, V = 4824.9(5) Å^3.

The formation of $NaBH_4$ is further confirmed by IR spectroscopy (Fig. S7, ESI†). The two B–H stretching bands at ∼2500 cm^{-1} from $Na_2B_{10}H_{10}$ in Na_2B_{10}-A are replaced by a single broad band at ∼2400 cm^{-1} in Na_2B_{10}-B, indicating that a different B–H containing cluster is formed, possibly a *closo*-, *arachno*-, or *nido*-borate, which could potentially be ascribed to the unidentified compound **2**. Finally, the two stretching modes between 2350–2250 cm^{-1} are assigned to $NaBH_4$.

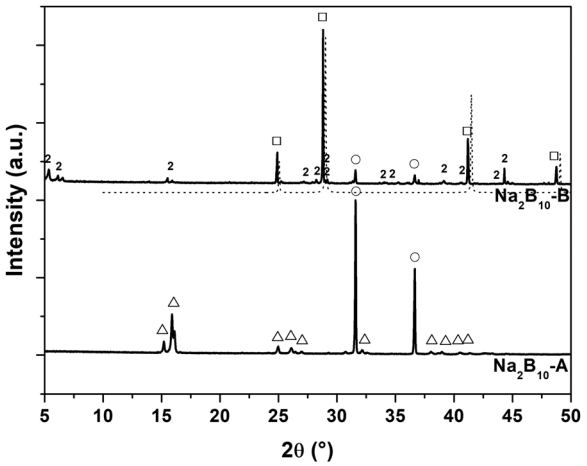

Fig. 4 Normalized powder X-ray diffraction patterns of $Na_2B_{10}H_{10}$–8NaH after manually grinding (Na_2B_{10}-A) and after hydrogenation (Na_2B_{10}-B) at T = 289 °C and $p(H_2)$ = 534 bar for 24 hours (λ = 1.54056 Å). Symbols: □ $NaBH_4$, ○ NaH, △ LT-$Na_2B_{10}H_{10}$, and compound **2**. The dotted pattern is that of pure $NaBH_4$, overlaid for comparison.

The hydrogenation of the composite $Na_2B_{10}H_{10}$–8NaH was investigated by HP *in situ* SR-PXD and the diffraction data is presented in Fig. 5. Initially, Bragg reflections from the reactants, $Na_2B_{10}H_{10}$ and NaH, are observed followed by the well-known α- to β-$Na_2B_{10}H_{10}$ polymorphic transition at $T \sim 130$ °C.[50] After 20 min at T = 302 °C and $p(H_2) \sim 440$ bar (t = 60 min), Bragg reflections from **2** are observed, whereas $NaBH_4$ is observed after approximately 220 minutes at T = 250 °C during cooling. This reaction time agrees well with the ∼4 hours induction time observed in *ex situ* hydrogen absorption in Fig. S5 (ESI†). Thus, **2** may represent an intermediate in the formation of $NaBH_4$ from the $Na_2B_{10}H_{10}$–8NaH composite.

The ^{11}B MAS NMR spectrum of Na_2B_{10}-B (Fig. 3b) reveals at least two different boron environments, with the dominating resonance at −41.9 ppm originating from $NaBH_4$.[51] The second broad resonance is centered at −28 ppm and includes a sharp low-intensity component at −30 ppm. The main component of the resonance at −28 ppm is ascribed to **2** while the sharp resonance at −30 ppm is ascribed to a small amount of the $Na_2B_{10}H_{10}$ starting material.[44] The molar ratio for boron in $NaBH_4$ and **2** of 1:0.21 and is derived from the intensities of the central and satellite transitions for $NaBH_4$ and the central transition for the −28 ppm resonance.

The ^{23}Na MAS NMR spectrum of the Na_2B_{10}-B sample (Fig. 6a) is dominated by resonances from $NaBH_4$ (−7.9 ppm) and NaH (18.2 ppm).[52] Spectral integration, considering the centerband intensities only, reveals that $NaBH_4$ and NaH are present in a 1:0.16 molar ratio. The vertical expansion of the spectrum (Fig. 6a) shows at least four additional resonances, *i.e.*, a second-order quadrupolar lineshape with singularities at 12.2 and 11.1 ppm, a broadened resonance at 2.7 ppm, a shoulder to the $NaBH_4$ centerband at −2.8 ppm and a resonance at −17.9 ppm. These additional resonances constitute 8.3% of the total intensity in the centerband region and thereby represent smaller amounts of other Na containing compounds, possibly **2**.

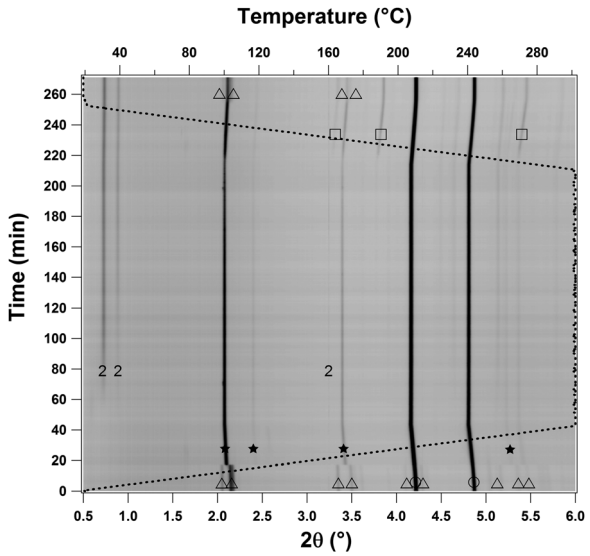

Fig. 5 *In situ* high pressure synchrotron powder X-ray diffraction patterns of the hydrogenation of $Na_2B_{10}H_{10}$–8NaH heated from RT to 302 °C, at $p(H_2)$ = 440 bar ($\Delta T/\Delta t$ = 10 °C min^{-1}, λ = 0.20720 Å). The sample was kept isothermal at T = 302 °C for ~3 hours. The dashed line indicates the temperature profile. Symbols: □ $NaBH_4$, ○ NaH, △ LT-$Na_2B_{10}H_{10}$, ★ HT-$Na_2B_{10}H_{10}$, and compound **2**.

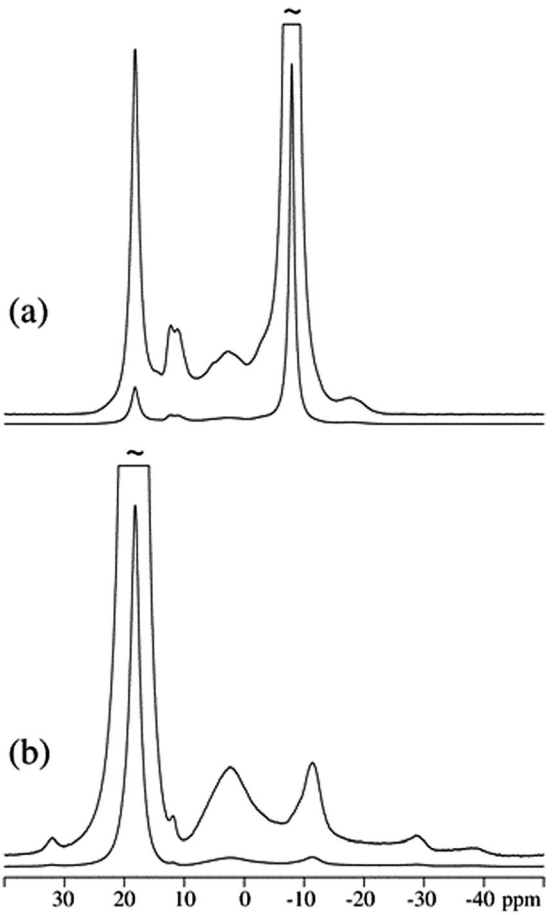

Fig. 6 ^{23}Na MAS NMR spectra (16.45 T, ν_R = 15.0 kHz) of the hydrogenated samples (a) Na_2B_{10}-B and (b) Na_2B_{12}-B. The spectra illustrate the spectral region for the central transitions and they are shown on normalized as well as expanded intensity scales.

Solution ^{11}B NMR spectra of Na_2B_{10}-B dissolved in THF and obtained with and without ^{1}H decoupling (Fig. 7) show resonances at −1.7 ppm ($^1J_{BH}$ = 134 Hz), −17.5 ppm ($^1J_{BH}$ = 125 Hz), −20.7 ppm ($^1J_{BH}$ = 125 Hz), −21.3 ppm ($^1J_{BH}$ = 125 Hz) and −29.9 ppm ($^1J_{BH}$ = 119 Hz), all corresponding to boron bonded to one H atom, and a main peak at −41.8 ppm from the $[BH_4]^-$ units. The peaks at −1.7 ppm and −29.9 ppm exhibit a 1 : 4 intensity ratio and are ascribed to the two distinct B sites in $[B_{10}H_{10}]^{2-}$, in accordance with ^{11}B NMR data from literature.[53] Thus, the resonances at −17.5 ppm, −20.7 ppm, and −21.3 ppm are assigned to **2** and is in accord with data reported for $[B_{11}H_{11}]^{2-}$ (Table S4, ESI†), which is a *closo*-borate with terminal hydrogens only, *i.e.*, B–H units producing doublets in liquid state NMR spectra.

Thus, the measured hydrogen uptake of 3.2 wt% H_2 corresponds to a sample composition of 10Na–10B–29.3H, and Na NMR reveals a sample composition of $NaBH_4$–NaH 1 : 0.16 and that $Na_2B_{11}H_{11}$ (denoted **2**) accounts for <8.3% of the sodium in the sample. Boron NMR reveals a ratio between $NaBH_4$–$Na_2B_{11}H_{11}$ of 1 : 0.21. The products besides $NaBH_4$ and $Na_2B_{11}H_{11}$ are difficult to determine and may be a mixture of different borates.

Hydrogenation of metal dodecahydro-*closo*-dodecaborate $M_2B_{12}H_{12}$–10MH compositions

Sample $Li_2B_{12}H_{12}$–10LiH. PXD of the physical mixture Li_2B_{12}-A is shown in Fig. 8. Li_2B_{12}-A was heated to T = 402 °C and kept isothermal for 24 hours at $p(H_2)_{start}$ = 546 bar. The total pressure decrease corresponds to a H_2 uptake of 2.19 wt% H_2. However, PXD of Li_2B_{12}-B reveals no changes in the composite except for weak reflections from Li_2O. Experiments conducted on $Li_2B_{12}H_{12}$–10LiH samples at high pressure, $p(H_2)$ = 970 bar and T = 400 °C for 48 h (Li_2B_{12}-C and Li_2B_{12}-D), confirmed that no $LiBH_4$ or other compounds were produced under the conditions used in this study (Fig. S9, ESI†). Hence, the pressure decrease observed in Fig. S8 (ESI†) is possibly due to a slight hydrogen gas leak.

This finding is further supported by the ^{11}B MAS NMR spectrum of Li_2B_{12}-B (Fig. S10a, ESI†) that almost exclusively shows a single resonance peak at −15.2 ppm, in agreement with the reported chemical shift for $Li_2B_{12}H_{12}$.[44]

Sample $Na_2B_{12}H_{12}$–10NaH. The physical mixture of $Na_2B_{12}H_{12}$–10NaH (Na_2B_{12}-A) was heated to T = 401 °C and kept isothermal for 24 hours at $p(H_2)$ = 537 bar (Fig. S11, ESI†). PXD of Na_2B_{12}-B (Fig. 9) reveals no formation of $NaBH_4$; however, another unidentified compound is observed, denoted **3**. The total pressure decrease corresponds to a H_2 uptake of 1.5 wt% H_2 (Fig. S11, ESI†). Experiments conducted on $Na_2B_{12}H_{12}$–10NaH samples at higher pressure, $p(H_2)$ = 970 bar and T = 400 °C for 48 h (Na_2B_{12}-C and Na_2B_{12}-D), confirmed that no $NaBH_4$ was produced (Fig. S12, ESI†); however, both samples show formation of **3**. The ball-milled sample, Na_2B_{12}-C, shows less remaining $Na_2B_{12}H_{12}$

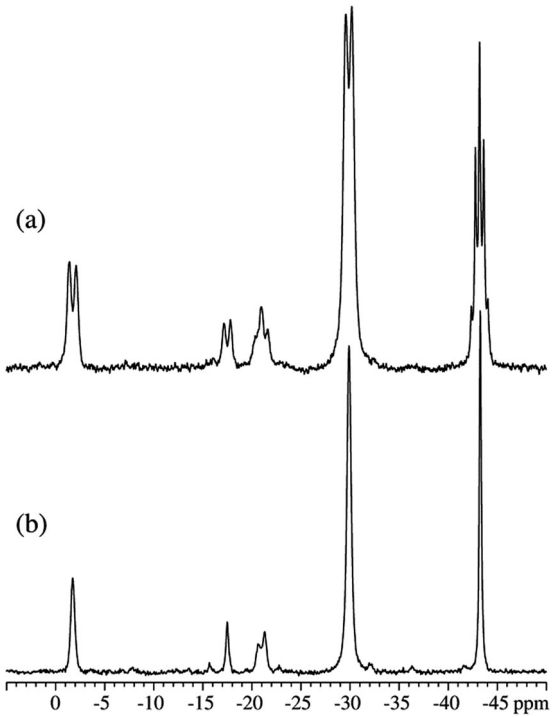

Fig. 7 Solution ^{11}B NMR spectra (14.1 T) of Na_2B_{10}-B dissolved in THF obtained (a) without and (b) with ^{1}H decoupling.

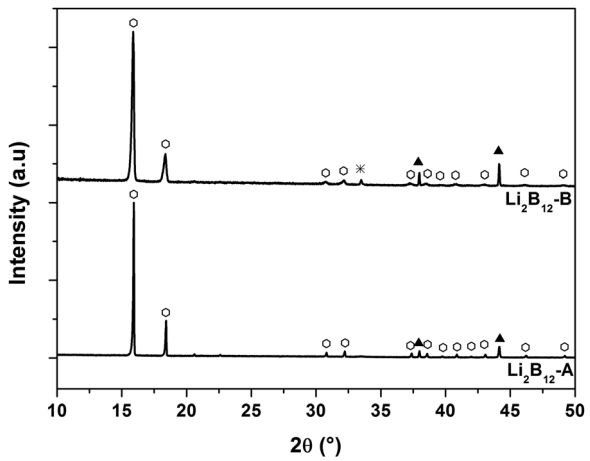

Fig. 8 Normalized powder X-ray diffraction patterns of $Li_2B_{12}H_{12}$–10LiH after manually grinding (Li_2B_{12}-A) and after hydrogenation (Li_2B_{12}-B) at T = 402 °C and $p(H_2)$ = 546 bar for 24 hours (λ = 1.54056 Å). Symbols: ⬡ LT-$Li_2B_{12}H_{12}$, ▲ LiH, and ✳ Li_2O.

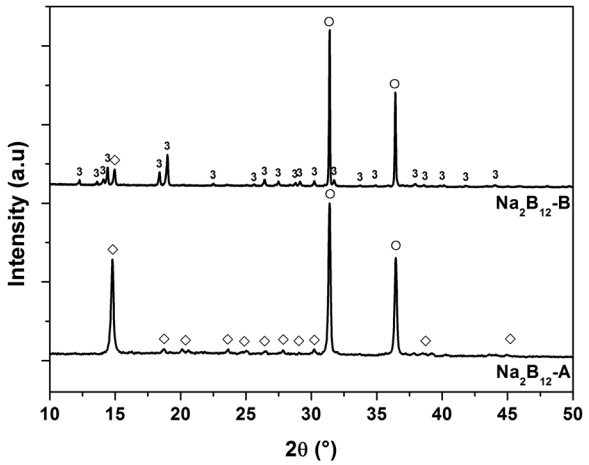

Fig. 9 Normalized powder X-ray diffraction patterns of $Na_2B_{12}H_{12}$–10NaH after manually grinding (Na_2B_{12}-A) and after hydrogenation (Na_2B_{12}-B) at T = 401 °C and $p(H_2)$ = 537 bar for 24 hours (λ = 1.54056 Å). Symbols: ◇ LT-$Na_2B_{12}H_{12}$, ○ NaH, and compound **3**.

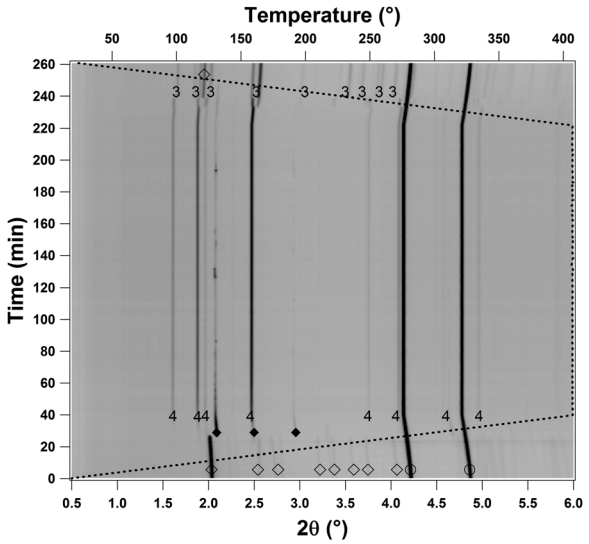

Fig. 10 *In situ* high pressure synchrotron powder X-ray diffraction patterns of the hydrogenation of $Na_2B_{12}H_{12}$–10NaH heated from RT to 407 °C, at $p(H_2)$ = 417 bar ($\Delta T/\Delta t$ = 10 °C min^{-1}, λ = 0.20720 Å). The sample was kept isothermal at T = 407 °C for ~3 hours. The dashed line indicates the temperature profile. Symbols: ◇ LT-$Na_2B_{12}H_{12}$, ◆ HT-$Na_2B_{12}H_{12}$, ○ NaH, compound **3**, and compound **4**.

compared to the hand-ground sample, Na_2B_{12}-D, probably due to a smaller particle size and hence a higher reactivity.

The change in structures is investigated by IR spectroscopy (Fig. S13, ESI†). The B–H stretching bands at ~2478 cm^{-1} from $Na_2B_{12}H_{12}$ in Na_2B_{12}-A are shifted slightly to a lower value of 2462 cm^{-1} in Na_2B_{12}-B, which may be ascribed to **3** along with a new bending mode at ~1650 cm^{-1}.

The formation of **3** is studied by HP *in situ* SR-PXD (Fig. 10). Initially, Bragg reflections from $Na_2B_{12}H_{12}$ and NaH are present, and, during heating, the polymorphic transition of α- to β-$Na_2B_{12}H_{12}$ is observed at ~275 °C.[54] In addition, an unidentified compound denoted **4** is observed. No changes in the diffraction pattern are observed at the isothermal temperature, but Bragg reflections from compound **4** disappear at T ~ 210 °C during cooling. At the same time, Bragg reflections from compound **3** appear, which indicates a phase transition of **4** into **3**. Reflections from compounds **3** and **4** are listed in Table S3 (ESI†) with the *d*-spacing and relative intensities. Indexing suggests an orthorhombic unit cell for **3**: a = 6.9114(6), b = 12.877(2), c = 14.296(1) Å, V = 1272.2(5) Å^3, and an orthorhombic unit cell for **4**: a = 6.3383(2), b = 10.5223(8), c = 14.8283(7) Å and V = 987.4(2) Å^3.

The ^{11}B MAS NMR spectrum of Na_2B_{12}-B (Fig. S10b, ESI†), exhibits a narrow resonance (full width at half maximum (FWHM) = 0.7 ppm) at −15.7 ppm, in accordance with the ^{11}B chemical shift reported for $Na_2B_{12}H_{12}$, which may suggest that **3** has boron coordination similar to that of $Na_2B_{12}H_{12}$.[44] PXD clearly shows the formation of a new crystalline product after hydrogenation at high temperature, whereas NMR results only indicate the presence of $[B_{12}H_{12}]^{2-}$-containing compounds. A previous study has shown that annealing $Li_2B_{12}H_{12}$ under hydrogen pressure can result in the formation of additional Bragg diffraction peaks, indicating that other compounds may form at high temperature.[55] Compound **3** appears to consist of $[B_{12}H_{12}]^{2-}$ anions as suggested by NMR.

The ^{23}Na MAS NMR spectrum of Na_2B_{12}-B (Fig. 6b) is dominated by a resonance at 18.2 ppm from NaH. In addition, minor peaks are observed at 32.1 ppm, 11.9 ppm, 2.3 ppm, −11.4 ppm, −28.8 ppm and −38 ppm. A ^{23}Na MAS NMR spectrum of $Na_2B_{12}H_{12}$ reveals that the resonance at −11.4 ppm originates from this compound. Moreover, the peaks at −28.8 ppm and −38 ppm are most likely the low-frequency part (singularity and edge) of a second-order quadrupolar lineshape. However, the resonances at 32.1 ppm, 11.9 ppm, 2.3 ppm, −28.8 ppm, and −38 ppm are not assigned and thus they may include contributions from the unidentified compound **3**. Spectral integration shows that the four resonances correspond to 10.7% of the total ^{23}Na centerband intensity.

The Na_2B_{12}-B sample absorbed 1.5 wt% H_2, which corresponds to a sample composition of 12Na–12B–28.4H. Solid state ^{11}B MAS NMR show that **3** has similar chemical environment as $[B_{12}H_{12}]^{2-}$ and diffraction reveal that **4** transforms to **3** upon cooling.

Comparison of the investigated *closo*-borate composites

Comparison of the reactivity of the Li and Na *closo*-borate composites, $Li_2B_{10}H_{10}$–8LiH and $Na_2B_{10}H_{10}$–8NaH, reveals several important differences. For instance, the Na composites have faster kinetics for hydrogenation than the corresponding Li samples, *e.g.*, Li_2B_{10}-A absorbs hydrogen slowly for the first 6 hours, then ∼5× faster for 8 hours and then again slower whereas Na_2B_{10}-A does not absorb hydrogen for the first 3 hours then absorbs quickly for 12 h, and then more slowly. From a kinetic point of view, the shorter induction period for the sodium system may be associated with faster nucleation and growth of intermediate compounds prior to formation of $NaBH_4$ as compared to similar reactions for the analogous lithium composites. This is well documented by solid-state ^{11}B NMR, which reveals sample compositions of $LiBH_4$–**1** (1 : 0.63) for $Li_2B_{10}H_{10}$–8LiH and $NaBH_4$–**2** (1 : 0.21) for $Na_2B_{10}H_{10}$–8NaH after 24 h. *In situ* HP SR-PXD experiments reveal the formation of $NaBH_4$ after 4 hours of $Na_2B_{10}B_{10}$–8NaH, whereas $LiBH_4$ forms after 10 hours. A major difference between composites based on $M_2B_{10}H_{10}$ and $M_2B_{12}H_{12}$ is their reactivity; those based on $M_2B_{10}H_{10}$ more readily form the corresponding metal borohydride, MBH_4, and intermediate compounds. In contrast, only unidentified compounds are observed in the $Na_2B_{12}H_{12}$–10NaH composite, whereas no reaction is observed for $Li_2B_{12}H_{12}$–10LiH under the conditions used in this study. Four different intermediate compounds have been observed during hydrogenation reactions in this investigation. However, they are different than intermediates predicted theoretically for the decomposition of $LiBH_4$ and to those observed experimentally.[36,56]

In a previous study, $Li_2B_{12}H_{12}$–10LiH and $Na_2B_{12}H_{12}$–10NaH were fully converted to the respective metal borohydrides, $LiBH_4$ and $NaBH_4$, under harsher conditions, *i.e.* T = 500 °C, $p(H_2)$ = 1.0 kbar for 72 h.[39] Milder conditions are used in this study, *i.e.* $T \sim 400$ °C, $p(H_2) \sim 998$ bar for 24 h for hydrogenation of $M_2B_{10}H_{10}$–8MH and $T \sim 400$ °C, $p(H_2) \sim 970$ bar for 48 h for $M_2B_{12}H_{12}$–10MH, which proves insufficient to form the respective metal borohydride. The $M_2B_{10}H_{10}$ composites are clearly more reactive and take up hydrogen at milder conditions compared to the $M_2B_{12}H_{12}$ composites, possibly due to the lower thermodynamic stability of the $[B_{10}H_{10}]^{2-}$ anion, which allows B–B bond breaking to occur under milder reaction conditions.

Conclusions

The composites $M_2B_{12}H_{12}$–10MH and $M_2B_{10}H_{10}$–8MH (M = Li and Na) have been reacted with hydrogen at elevated pressures and temperatures and studied by X-ray diffraction both PXD and *in situ* SR-PXD and FT-IR, ^{23}Na and ^{11}B NMR spectroscopy. Both the *in situ* and *ex situ* characterization results show that the $M_2B_{10}H_{10}$–8MH composites react with hydrogen gas to form the respective metal borohydride, MBH_4, at $T \sim 300$ °C and $p(H_2) > 500$ bar. These conditions were deliberately selected to obtain partial hydrogenation of the samples in order to focus on the mechanism of hydrogen uptake. The relatively mild conditions used in this investigation did not allow formation of MBH_4 by hydrogenation of the $M_2B_{12}H_{12}$–10MH composites: no hydrogen absorption was detected for $Li_2B_{12}H_{12}$–10LiH, but new intermediates were observed for $Na_2B_{12}H_{12}$–10NaH. Generally, the sodium-containing composites are observed to be more reactive towards hydrogen compared to the lithium analogues under similar conditions of temperature and H_2 pressure, and $M_2B_{10}H_{10}$–8MH are more reactive than $M_2B_{12}H_{12}$–10MH. The high stability of the $[B_{12}H_{12}]^{2-}$ anions is associated with the pseudoaromatic bonding in dodecahydro-*closo*-dodecaborate cages and lack of chemically distinct and more reactive apical boron atoms within the *closo*-borate polyhedra that the decahydro-*closo*-decaborate cages contain.

The conditions for hydrogenation used in this study are clearly above the thermodynamic limit needed to form the corresponding metal borohydrides, $LiBH_4$ or $NaBH_4$, for the composites containing $[B_{10}H_{10}]^{2-}$. Therefore, the observed differences in the length of the induction periods prior to hydrogen absorption, which occur at different rates, are assigned to kinetic constraints. Remarkably, four different intermediate compounds have been observed in this study for the hydrogenation of the composites. The formation of intermediate compounds appears to be the rate-limiting step of the

reaction, with the slowest kinetics observed for the $M_2B_{12}H_{12}$ compounds. This suggest that the molecular mechanism for hydrogen absorption is different for the two *closo*-borate cages, $[B_{10}H_{10}]^{2-}$ and $[B_{12}H_{12}]^{2-}$.

This study not only demonstrates that lithium and sodium $M_2B_{10}H_{10}$ salts can be hydrogenated into the corresponding metal borohydrides, but it also reveals the presence of, at least, four B–H intermediates, which are different to those previously observed experimentally or suggested based on theoretical calculations. Additional investigations are needed to clarify composition, structure, and properties of these intermediate compounds. The analysis of the available solid-state and solution ^{11}B NMR data indicates that these intermediates are not salts of $[B_3H_8]^-$, $[B_{10}H_{10}]^{2-}$ or $[B_{12}H_{12}]^{2-}$ anions. We hypothesize that these could be other *closo*-polyborates, *e.g.*, $[B_9H_9]^{2-}$ or $[B_{11}H_{11}]^{2-}$ salts, or oligomers resulting from $[B_{10}H_{10}]^{2-}$ polymerization.[29] For example, *closo*-decaborate salts are known to form dimeric anions, such as various isomers of $[B_{20}H_{18}]^{4-}$ and $[B_{20}H_{18}]^{2-}$ anions.[57]

A detailed understanding of the reactivity of these important compounds may allow further tailoring of the reaction mechanisms of hydrogen storage reactions. Further investigations should focus on identifying reaction pathways in the dehydrogenation of metal borohydrides that avoid the formation of stable $[B_{12}H_{12}]^{2-}$ anions, and favoring formation of intermediate B–H species that can be cycled under more reasonable conditions of hydrogen pressure and temperature.

Conflicts of interest

There are no conflicts to declare.

Acknowledgements

The Danish National Research Foundation is thanked for funding to the Center for Materials Crystallography (CMC, DNRF93). Furthermore, we acknowledge financial support from The Danish Council for Independent Research for a DFF Mobility grant (no. 1325-00072) and the research project HyNanoBorN (DFF – 4181-00462). The beam line P02.1, PETRA III, DESY, Germany is acknowledged for providing beam time to conduct the *in situ* experiments. The use of the facilities at the Instrument Centre for Solid-State NMR Spectroscopy, Aarhus University, sponsored by the Danish Natural Science Research Councils and the Carlsberg Foundation is acknowledged. The authors gratefully acknowledge research support from the U.S. Department of Energy, Office of Energy Efficiency and Renewable Energy, Fuel Cell Technologies Office through the Hydrogen Storage Materials Advanced Research Consortium (HyMARC). Sandia National Laboratories is a multi-mission laboratory managed by National Technology and Engineering Solutions of Sandia, LLC, a wholly owned subsidiary of Honeywell International Inc., for the U.S. Department of Energy's National Nuclear Security Administration under contract DE-NA0003525. This paper describes objective technical results and analyses. Any subjective views or opinions that might be expressed in the paper do not necessarily represent the views of the U.S. Department of Energy or the United States Government.

References

1 The Relentless Rise of Carbon Dioxide, http://climate.nasa.gov/climate_resources/24/, accessed October 2nd, 2017.
2 U. S. EIA, International Energy Outlook, 2016, http://www.eia.gov/forecasts/ieo/pdf/0484(2016).pdf.
3 M. B. Ley, L. H. Jepsen, Y.-S. Lee, Y. W. Cho, J. M. Bellosta von Colbe, M. Dornheim, M. Rokni, J. O. Jensen, M. Sloth, Y. Filinchuk, J. E. Jørgensen, F. Besenbacher and T. R. Jensen, *Mater. Today*, 2014, **17**, 122–128.
4 L. H. Jepsen, M. B. Ley, Y.-S. Lee, Y. W. Cho, M. Dornheim, J. O. Jensen, Y. Filinchuk, J. E. Jørgensen, F. Besenbacher and T. R. Jensen, *Mater. Today*, 2014, **17**, 129–135.
5 K. T. Møller, T. R. Jensen, E. Akiba and H.-W. Li, *Prog. Nat. Sci.: Mater. Int.*, 2017, **27**, 34–40.
6 H.-W. Li, Y. Yan, S. Orimo, A. Züttel and C. M. Jensen, *Energies*, 2011, **4**, 185–214.
7 J. Puszkiel, S. Garroni, C. Milanese, F. Gennari, T. Klassen, M. Dornheim and C. Pistidda, *Inorganics*, 2017, **5**.
8 G. Moussa, R. Moury, U. B. Demirci, T. Şener and P. Miele, *Int. J. Energy Res.*, 2013, **37**, 825–842.
9 M. Paskevicius, L. H. Jepsen, P. Schouwink, R. Cerny, D. B. Ravnsbaek, Y. Filinchuk, M. Dornheim, F. Besenbacher and T. R. Jensen, *Chem. Soc. Rev.*, 2017, **46**, 1565–1634.
10 G. Severa, E. Rönnebro and C. M. Jensen, *Chem. Commun.*, 2010, **46**, 421–423.
11 O. Friedrichs, J. W. Kim, A. Remhof, F. Buchter, A. Borgschulte, D. Wallacher, Y. W. Cho, M. Fichtner, K. H. Oh and A. Züttel, *Phys. Chem. Chem. Phys.*, 2009, **11**, 1515–1520.
12 M. Paskevicius, M. B. Ley, D. A. Sheppard, T. R. Jensen and C. E. Buckley, *Phys. Chem. Chem. Phys.*, 2013, **15**, 19774–19789.
13 P. Martelli, R. Caputo, A. Remhof, P. Mauron, A. Borgschulte and A. Züttel, *J. Phys. Chem. C*, 2010, **114**, 7173–7177.
14 Q. Lai, M. Paskevicius, D. A. Sheppard, C. E. Buckley, A. W. Thornton, M. R. Hill, Q. Gu, J. Mao, Z. Huang, H. K. Liu, Z. Guo, A. Banerjee, S. Chakraborty, R. Ahuja and K. F. Aguey-Zinsou, *ChemSusChem*, 2015, **8**, 2789–2825.
15 T. D. Humphries, M. B. Ley, C. Frommen, K. T. Munroe, T. R. Jensen and B. C. Hauback, *J. Mater. Chem. A*, 2015, **3**, 691–698.
16 P. Schouwink, M. B. Ley, A. Tissot, H. Hagemann, T. R. Jensen, L. Smrcok and R. Cerny, *Nat. Commun.*, 2014, **5**, 5706–5715.
17 M. B. Ley, M. Paskevicius, P. Schouwink, B. Richter, D. A. Sheppard, C. E. Buckley and T. R. Jensen, *Dalton Trans.*, 2014, **43**, 13333–13342.
18 P. Schouwink, V. D'Anna, M. B. Ley, L. M. Lawson Daku, B. Richter, T. R. Jensen, H. Hagemann and R. Černý, *J. Phys. Chem. C*, 2012, **116**, 10829–10840.
19 I. Lindemann, R. Domenech Ferrer, L. Dunsch, Y. Filinchuk, R. Cerny, H. Hagemann, V. D'Anna, L. M. Lawson Daku,

L. Schultz and O. Gutfleisch, *Chem. – Eur. J.*, 2010, **16**, 8707–8712.
20 R. Černý, P. Schouwink, Y. Sadikin, K. Stare, L. Smrcok, B. Richter and T. R. Jensen, *Inorg. Chem.*, 2013, **52**, 9941–9947.
21 R. Černý and P. Schouwink, *Acta Crystallogr., Sect. B: Struct. Sci.*, 2015, **71**, 619–640.
22 E. Roedern and T. R. Jensen, *Inorg. Chem.*, 2015, **54**, 10477–10482.
23 S. R. H. Jensen, L. H. Jepsen, J. Skibsted and T. R. Jensen, *J. Phys. Chem. C*, 2015, **119**, 27919–27929.
24 J. J. Vajo and S. L. Skeith, *J. Phys. Chem. B*, 2005, **109**, 3719–3722.
25 B. Sakintuna, F. Lamari-Darkrim and M. Hirscher, *Int. J. Hydrogen Energy*, 2007, **32**, 1121–1140.
26 C. J. Webb, *J. Phys. Chem. Solids*, 2015, **84**, 96–106.
27 J. Wang, H.-W. Li and P. Chen, *MRS Bull.*, 2013, **38**, 480–487.
28 B. R. S. Hansen, M. Paskevicius, H.-W. Li, E. Akiba and T. R. Jensen, *Coord. Chem. Rev.*, 2016, **323**, 60–70.
29 Y. Yan, A. Remhof, D. Rentsch and A. Züttel, *Chem. Commun.*, 2015, **51**, 700–702.
30 B. R. Hansen, D. B. Ravnsbaek, J. Skibsted and T. R. Jensen, *Phys. Chem. Chem. Phys.*, 2014, **16**, 8970–8980.
31 V. Stavila, J.-H. Her, W. Zhou, S.-J. Hwang, C. Kim, L. A. M. Ottley and T. J. Udovic, *J. Solid State Chem.*, 2010, **183**, 1133–1140.
32 O. Friedrichs, A. Remhof, S. J. Hwang and A. Züttel, *Chem. Mater.*, 2010, **22**, 3265–3268.
33 M. Chong, A. Karkamkar, T. Autrey, S. Orimo, S. Jalisatgi and C. M. Jensen, *Chem. Commun.*, 2011, **47**, 1330–1332.
34 K. C. Kim, A. D. Kulkarni, J. K. Johnson and D. S. Sholl, *Phys. Chem. Chem. Phys.*, 2011, **13**, 7218–7229.
35 S. V. Alapati, J. Karl Johnson and D. S. Sholl, *Phys. Chem. Chem. Phys.*, 2007, **9**, 1438–1452.
36 Z. Q. Huang, W. C. Chen, F. C. Chuang, E. H. Majzoub and V. Ozolins, *Sci. Rep.*, 2016, **6**, 26056.
37 V. Ozolins, E. H. Majzoub and C. Wolverton, *J. Am. Chem. Soc.*, 2009, **131**, 230–237.
38 Y. Zhang, E. Majzoub, V. Ozoliņš and C. Wolverton, *J. Phys. Chem. C*, 2012, **116**, 10522–10528.
39 J. L. White, R. J. Newhouse, J. Z. Zhang, T. J. Udovic and V. Stavila, *J. Phys. Chem. C*, 2016, **120**, 25725–25731.
40 B. R. S. Hansen, K. T. Møller, M. Paskevicius, A.-C. Dippel, P. Walter, C. J. Webb, C. Pistidda, N. Bergemann, M. Dornheim, T. Klassen, J.-E. Jørgensen and T. R. Jensen, *J. Appl. Crystallogr.*, 2015, **48**, 1234–1241.
41 E. L. Muetterties, J. H. Balthis, Y. T. Chia, W. H. Knoth and H. C. Muller, *Inorg. Chem.*, 1964, **3**, 444–451.
42 M. Paskevicius, D. A. Sheppard and C. E. Buckley, *J. Am. Chem. Soc.*, 2010, **132**, 5077–5083.
43 H. I. Schlesinger and H. C. Brown, *J. Am. Chem. Soc.*, 1940, **62**, 3429–3435.
44 L. He, H.-W. Li and E. Akiba, *Energies*, 2015, **8**, 12429–12438.
45 N. N. Greenwood and A. Earnshaw, *Chemistry of the Elements*, Elsevier Ltd, 2nd edn, 1997.
46 M. Sharma, D. Sethio, V. D'Anna and H. Hagemann, *Int. J. Hydrogen Energy*, 2015, **40**, 12721–12726.
47 E. L. Muetterties, R. E. Merrifield, H. C. Miller, W. H. Knoth and J. R. Downing, *J. Am. Chem. Soc.*, 1962, **84**, 2506–2508.
48 H. Hagemann, http://www.unige.ch/sciences/chifi/?ftirdb.html.
49 V. D'Anna, A. Spyratou, M. Sharma and H. Hagemann, *Spectrochim. Acta, Part A*, 2014, **128**, 902–906.
50 T. J. Udovic, M. Matsuo, W. S. Tang, H. Wu, V. Stavila, A. V. Soloninin, R. V. Skoryunov, O. A. Babanova, A. V. Skripov, J. J. Rush, A. Unemoto, H. Takamura and S. Orimo, *Adv. Mater.*, 2014, **26**, 7622–7626.
51 A. C. Stowe, W. J. Shaw, J. C. Linehan, B. Schmid and T. Autrey, *Phys. Chem. Chem. Phys.*, 2007, **9**, 1831–1836.
52 R. Tabeta, M. Aida and H. Saitô, *Bull. Chem. Soc. Jpn.*, 1986, **59**, 1957–1966.
53 N. N. Greenwood and J. H. Morris, *Proc. Chem. Soc.*, 1963, 338–340, DOI: 10.1039/PS9630000325.
54 N. Verdal, J.-H. Her, V. Stavila, A. V. Soloninin, O. A. Babanova, A. V. Skripov, T. J. Udovic and J. J. Rush, *J. Solid State Chem.*, 2014, **212**, 81–91.
55 M. P. Pitt, M. Paskevicius, D. H. Brown, D. A. Sheppard and C. E. Buckley, *J. Am. Chem. Soc.*, 2013, **135**, 6930–6941.
56 L. Mosegaard, B. Møller, J.-E. Jørgensen, U. Bösenberg, M. Dornheim, J. C. Hanson, Y. Cerenius, G. Walker, H. J. Jakobsen, F. Besenbacher and T. R. Jensen, *J. Alloys Compd.*, 2007, **446–447**, 301–305.
57 M. F. Hawthorne, K. Shelly and F. Li, *Chem. Commun.*, 2002, 547–554.